nature nanotechnology

LETTERS

PUBLISHED ONLINE: 14 FEBRUARY 2010 | DOI: 10.1038/NNANO.2010.6

A diamond nanowire single-photon source

Thomas M. Babinec[1], Birgit J. M. Hausmann[1,2], Mughees Khan[1], Yinan Zhang[1], Jeronimo R. Maze[3], Philip R. Hemmer[4] and Marko Lončar[1]*

The development of a robust light source that emits one photon at a time will allow new technologies such as secure communication through quantum cryptography[1]. Devices based on fluorescent dye molecules[2], quantum dots[3] and carbon nanotubes[4] have been demonstrated, but none has combined a high single-photon flux with stable, room-temperature operation. Luminescent centres in diamond[5–9] have recently emerged as a stable alternative, and, in the case of nitrogen-vacancy centres, offer spin quantum bits with optical readout[10–15]. However, these luminescent centres in bulk diamond crystals have the disadvantage of low photon out-coupling. Here, we demonstrate a single-photon source composed of a nitrogen-vacancy centre in a diamond nanowire, which produces ten times greater flux than bulk diamond devices, while using ten times less power. This result enables a new class of devices for photonic and quantum information processing based on nanostructured diamond, and could have a broader impact in nanoelectromechanical systems, sensing and scanning probe microscopy.

It is well known that light–matter interactions, and in particular in- and out-coupling of photons, can be engineered by embedding emitters such as the nitrogen-vacancy (NV) centre (Fig. 1a) within nanophotonic structures. One approach currently under investigation is to evanescently couple a separate optical cavity or a waveguide to a proximal NV centre[16–20]. Although this scenario uses mature fabrication schemes, light–matter interactions are reduced by the displacement of the NV centre from the field maximum inside the device. Another approach is to realize optical structures directly in thin diamond films grown on foreign (low-index or sacrificial) substrates. Only polycrystalline diamond films are presently available, however, and their optical properties are inferior to those of single-crystal diamond[21]. Finally, devices may be sculpted from a bulk diamond crystal[22–26], but fabricating free-standing structures such as planar photonic crystals or microdisk resonators is a challenge.

The approach taken in this Letter is to apply top-down nanofabrication techniques to define large arrays of vertically oriented nanowire antennas in a single-crystal diamond substrate (Fig. 1b). Briefly, structures were made from a commercially available Type Ib diamond crystal. Electron-beam lithography and reactive-ion etching (RIE) were then used to realize ~200-nm-diameter, ~2-μm-long diamond nanowires with straight, smooth sidewalls (Fig. 1c). NV centres are embedded randomly in fabricated devices because the diamond substrate has a background of natural NV centres that are created during the crystal growth process. As a result, the etching process mechanically isolates individual NV centres and minimizes background fluorescence. This simple approach is a major advantage of the nanowire platform and is critical for this nascent material system. Fabrication details are provided in the Methods and elsewhere[26].

Three-dimensional finite-difference time-domain (FDTD) calculations predict that a nanowire antenna improves the performance of an NV centre single-photon source in two major ways. First, coupling optical power from a pump laser to a nanowire waveguide with an embedded NV centre allows for an order of magnitude more efficient excitation than in bulk diamond crystal. Second, the nanowire modifies the NV centre far-field emission and facilitates collection of emitted photons with an objective lens. For example, the fundamental nanowire mode (HE_{11}) is the dominant emission channel for an s-polarized dipole positioned on the nanowire axis (Fig. 1d)[27], and in this case light is emitted vertically from the top nanowire facet. On the other hand, a p-polarized dipole cannot emit into the waveguide mode due to the symmetry mismatch, but it can still emit into vertically propagating radiation modes (Fig. 1e). Because the NV centre dipole is polarized in the (111) plane of a (100) diamond nanowire[28,29], contributions of both s- and p-components need to be taken into account (see Methods). Finally, the fluorescence lifetime of an NV centre in a diamond nanowire is expected to be intermediate between that of bulk diamond, in which the NV centre lifetime is short (~12 ns) owing to the large background refractive index ($n \approx 2.4$), and that of an NV centre in a diamond nanoparticle (~25 ns), which resembles a dipole in air ($n \approx 1$)[9,26,27]. Furthermore, we find that the nanowire geometry allows for ~40% of emitted photons to be collected, compared to ~3% in the case of bulk. Finally, when modification of lifetime is taken into account, approximately an order of magnitude higher single-photon flux should be observed in a nanowire compared with the bulk (see Methods).

The diamond nanowires were optically addressed with a home-built laser scanning confocal microscope (Fig. 2a,b). A high-throughput screening technique was first used to scan large arrays of devices and to identify those showing the highest count rates (Fig. 2c). The device properties could then be studied over long periods of time (days) owing to the structural stability of the diamond nanowire and photostability of the embedded NV centre (Fig. 2d). For quantum device applications, we have verified the non-classical nature of light emitted from the diamond nanowire device. Single photons from an NV centre coupled to the nanowire antenna were sent one-by-one through a 50/50 beamsplitter, and were detected using an avalanche photodiode (APD) at each output channel (Hanbury Brown and Twiss configuration). The number of coincidence counts on each channel were measured as a function of the time delay τ and normalized to the Poissonian source[9] to give the corresponding intensity autocorrelation function $g^{(2)}(\tau)$. Strong photon antibunching ($g^{(2)}(0) < 1/2$) indicates that coupling between one NV centre and the nanowire antenna dominates over all other background sources, including stray light, APD dark counts and substrate fluorescence (Fig. 3a). At high pump powers, bunching ($g^{(2)}(\tau) > 1$) is observed at intermediate delay times due to optical cycling through a long-lived, non-radiative shelving state (Fig. 3b,c)[9]. In addition, the main features of the level-crossing system that lead to the polarization mechanism of

[1]School of Engineering and Applied Science, Harvard University, Cambridge, Massachusetts 02138, USA, [2]Department of Physics, Technische Universität München, D-85748 Garching, Germany, [3]Department of Physics, Harvard University, Cambridge, Massachusetts 02138, USA, [4]Department of Electrical and Computer Engineering, Texas A&M University, College Station, Texas 77843, USA. *e-mail: loncar@seas.harvard.edu

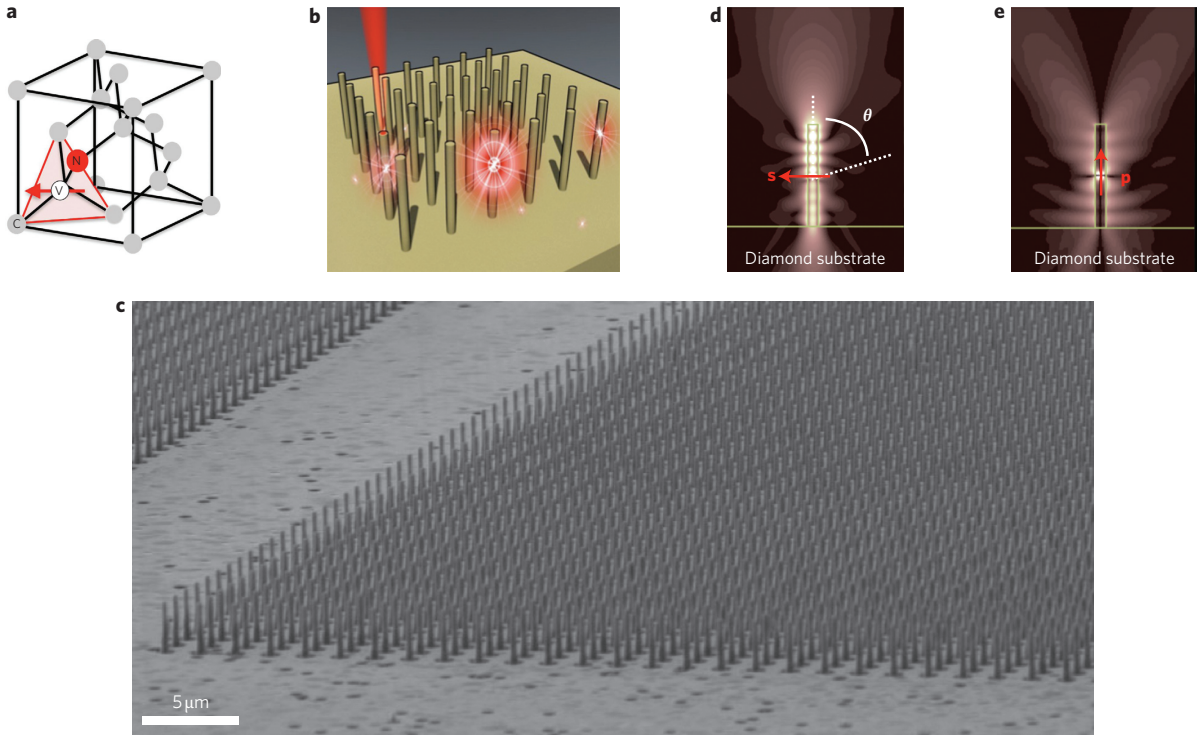

Figure 1 | Single-photon source based on an NV centre in a diamond nanowire. a, Schematic of the NV centre, which consists of an adjacent substitutional nitrogen atom and lattice vacancy in the diamond lattice. Broadband single-photon emission is due to a dipole transition that is polarized in the (111) crystal plane[28,29] (shaded triangle). **b**, Schematic representation of the device platform based on diamond crystal with randomly distributed NV centres (illustrated with light red dots). Photons emitted from the NV centre embedded within the nanowire are directed towards collection optics. **c**, Scanning electron microscope (SEM) image of a large array of fabricated diamond nanowire antennas. **d**, Representative field profile of a radial component of the *E*-field (E_r) in the case of a 2-μm-long, 200-nm-diameter diamond nanowire with an on-axis s-polarized dipole emitting at $\lambda = 637$ nm (zero-phonon line wavelength of NV centre), positioned at the nanowire centre. The fundamental nanowire waveguide mode (HE_{11}) is the dominant decay channel for the s-polarized dipole. Highly directional emission from the nanowire's top facet, contained within the collection angle (NA ≈ 0.95; $\theta \approx 72^{\circ}$) of an objective lens positioned above the nanowire, allows ~100% of the vertically emitted photons to be collected. **e**, Representative E_r field profile for the same device, but with a p-polarized dipole (vertical red arrow) positioned on the nanowire axis. Emission into upward propagating radiation modes still allows for significant collection from an objective lens.

the $m_s = 0$ sublevel of the triplet ground state and the spin-dependent fluorescence rate[30] remain unchanged after nanostructuring. This was confirmed by standard electron spin resonance and Rabi measurements (data not shown).

The fluorescence lifetime of a colour centre in the diamond nanowire gives an upper bound on the number of single photons that may be collected. This is encoded in the temporal width of the autocorrelation data, the exponential decay of which is of the form $\exp(-(r+\Gamma)|\tau|)$ for low pump powers[8,9]. Here, r is the pump rate, $\Gamma = 1/\tau_{NW}$ is the NV centre decay rate, and τ_{NW} is the NV centre lifetime in the nanowire. The overall decay rate $r + \Gamma$ was measured at different pump powers and observed to decrease linearly at low pump powers (Fig. 3d). The lifetime of six different nanowire devices was observed to be in the range $\tau_{NW} = 14.6 \pm 1.9$ ns, which is slightly longer than the lifetime of an NV centre in a bulk material, as expected.

The dramatic benefits of nanostructuring are most directly observed by comparing the single photon flux from an individual NV centre in a nanowire one in a bulk crystal. The key device parameters are P_{sat}, which is a measure of how much optical power must be used to saturate the NV centre response, and I_{sat}, which is the number of single photon counts per second (cps) that may be collected from the device. These parameters were extracted from a measurement of the device count rate for different pump powers. After a sharp rise at low pump powers ($P < P_{sat}$), the number of collected photons per second saturated at high powers (I_{sat}) due to the finite NV centre emission rate according to[8] $I(P) = I_{sat}/(1 + P_{Sat}/P)$. This single photon L–L curve is shown for a representative bulk NV device in Fig. 4a, demonstrating $I_{sat} = 21 \pm 2$ kcps and $P_{sat} = 990 \pm 540$ μW. The result for a typical nanowire device is likewise shown in Fig. 4b, in which device performance is given by $I_{sat} = 168 \pm 37$ kcps and $P_{sat} = 58 \pm 37$ μW. This corresponds to $\sim 2.5 \times 10^{-4}$ collected photons per NV centre lifetime in the bulk device and $\sim 2.5 \times 10^{-3}$ in the nanowire antenna. Factors such as optical cycling through the metastable shelving state and, more importantly, losses in the optical system used in the experiment, are the reason that the absolute photon counts measured in our devices deviate from the theoretical predictions. However, a relative comparison between photon counts obtained from the diamond nanowire and bulk diamond, shown in Fig. 4c (I_{sat} versus P_{sat}), is insensitive to these imperfections and unambiguously demonstrates the order of magnitude more efficient in- and out-coupling of light in the case of nanowire geometry.

For the first time, we have used a top-down nanofabrication technique to enhance the optical properties of an individual colour centre in single-crystal diamond. The fabrication technique retains the crucial properties of an NV centre, and is compatible with the requirements needed for the realization of scalable quantum systems based on diamond. Further fundamental studies of the properties of an NV centre in diamond nanostructures will facilitate their integration into more complex photonic quantum information devices, in which more advanced functions such as increasing the photon production rate by means of the Purcell effect will allow devices operating at even higher count levels and lower powers.

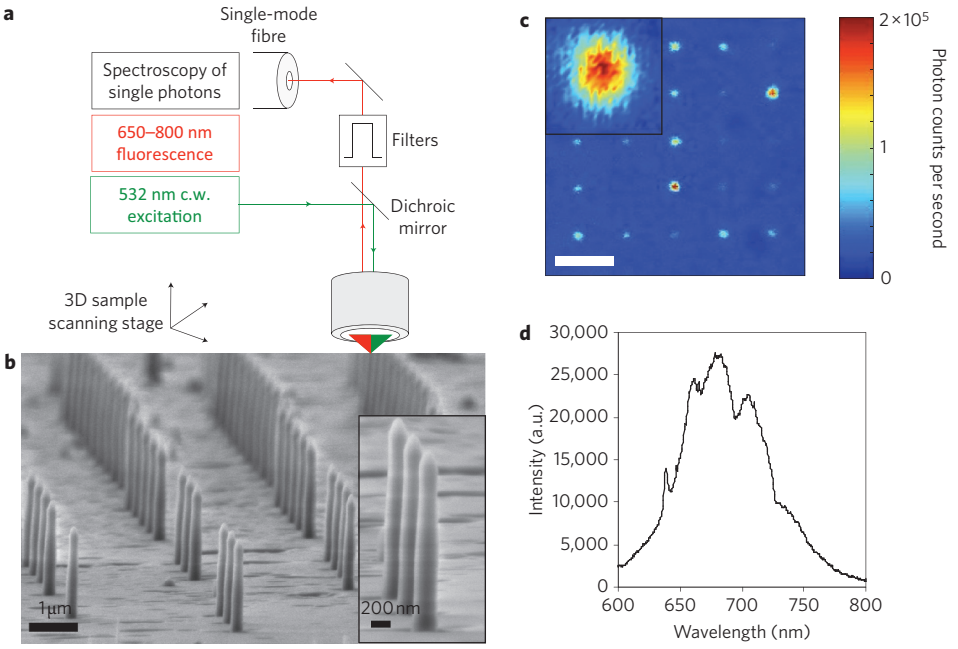

Figure 2 | Confocal microscopy of an array of diamond nanowires containing NV centres. a, The room-temperature scanning confocal microscope used in this experiment consists of a 532 nm c.w. laser used to excite the NV centre, a dichroic mirror to spectrally separate the red NV centre fluorescence, and a single-mode fibre acting as a confocal pinhole to reject unfocused light. An air objective lens with NA = 0.95 is used to focus the pump green light onto the sample and collect emitted red photons. **b**, An SEM micrograph showing an array of the typical ~200-nm-diameter nanowires analysed in this experiment. **c**, Confocal microscope image of a square array of nanowire devices (scale bar, 5 μm). Light blue and yellow spots correspond to nanowires with no embedded NV centre and nanowires containing a weakly coupled NV centre (for example, off-axis NV centres), respectively. Single-photon sources with the best performance appear red in this image due to their high photon count rates. The inset shows an enlarged image of one of the nanowire devices. **d**, Photoluminescence spectrum of photons collected from a typical diamond nanowire, showing the NV centre zero-phonon line at ~637 nm and phonon sideband from 640 to 780 nm.

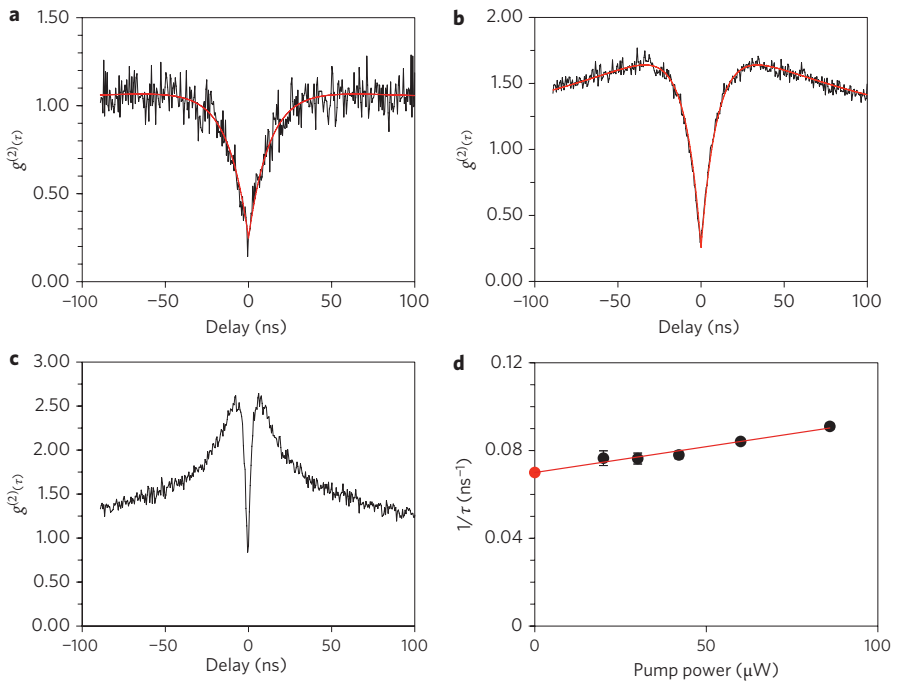

Figure 3 | Non-classical light emission from an NV centre in a diamond nanowire. a–c, The presence of a single quantum emitter in the diamond nanowire is revealed by the second-order autocorrelation function $g^{(2)}(\tau)$. The dramatic decrease at zero time delay ($g^{(2)}(0) < 1/2$) indicates that photons from the nanowire device are anti-bunched. Qualitatively different dynamics are observed at different excitation powers: 11 μW, below saturation (**a**); 190 μW, at saturation (**b**); and 1.6 mW, above saturation (**c**). At high pump powers, coupling to the metastable shelving state is significant and results in bunching shoulders ($g^{(2)}(\tau) > 1$) at intermediate times. The red curves in **a** and **b** are fits using a three-level model of the $g^{(2)}(\tau)$ function[8]. **d**, The decay rate of the $g^{(2)}(\tau)$ spectrum measured for different excitation conditions gives the fluorescence lifetime in the limit of zero pump power[9]. This extrapolation yields a lifetime of $\tau_{NW} = 14.0$ ns for this NV–nanowire system, which is slightly larger than that of bulk material (11.8 ns). This is consistent with the slight suppression of emission in nanowires predicted by the numerical model. Error bars represent ±1 standard error in the decay rate fitting parameter.

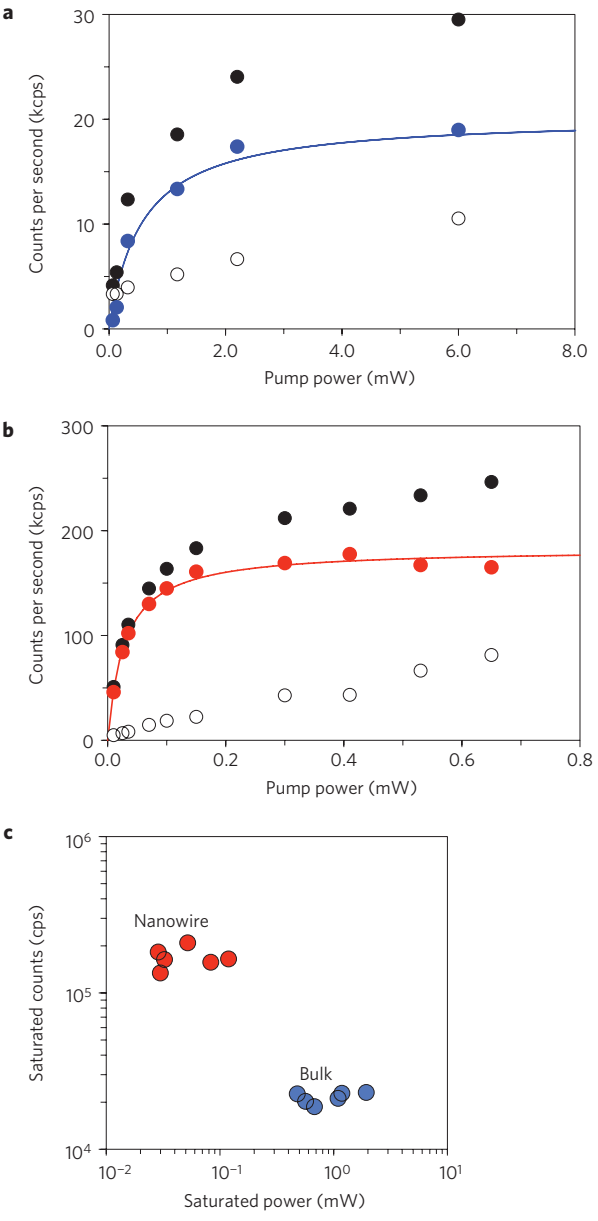

Figure 4 | Comparison between diamond nanowire and bulk diamond crystal single-photon sources. a,**b**, The number of single photons per second collected from a single NV centre in an ultrapure bulk diamond crystal (**a**) and in a diamond nanowire (**b**). Laser pump power incident on the objective is quoted. Black circles indicate raw count data from the device, hollow circles show the linear background data measured from the device, and coloured circles show the net NV centre counts. The NV centre single-photon *L*–*L* curves are fitted using the saturation model described in the text. **c**, Distribution of the single-photon device properties for the bulk diamond devices and diamond nanowire antennas tested in this experiment. Nanowire devices are pumped an order of magnitude more efficiently (*x* axis) than bulk devices and allow for an order of magnitude higher single-photon flux (*y* axis).

Finally, by implanting colour centres in nanowires fabricated in ultrapure diamond, simultaneous optimization of both spin and optical properties will be possible in a single device.

Methods

Device fabrication. The nanowire devices used in this experiment were prepared from a high-pressure, high-temperature, Type Ib diamond, the top surface of which was cut along the (100) crystal plane (Element 6 Corporation). The diamond was first cleaned in a boiling 1:1:1 nitric, perchloric and sulphuric acid bath to remove surface contamination. A 1:2 dilution of FOx 17 negative electron-beam resist with methyl isobutyl ketone (MIBK) was then spun on the diamond to form the resist layer. Arrays of ~200-nm-diameter circles were then patterned using an Elionix electron-beam writing system at a dosage of ~6,000 μC cm^{-2}. Tetra-methyl ammonium hydroxide (TMAH, 25%) was used to develop the resist and form the etch mask. The diamond crystal was then placed in an inductively coupled plasma (ICP) reactive-ion etching (RIE) system and etched for 10 min with 30 s.c.c.m. of oxygen gas, 100 W bias power at a chamber pressure of 10 mtorr. For the first 2 min, 700 W ICP power was applied, then 3 min of 600 W ICP power, and finally 5 min of 1,000 W ICP power, resulting in vertical nanowire structures with lengths of ~2.0 μm. An HF wet etch was used to remove the mask from the top of the nanowires, and an additional acid bath treatment was performed before device testing.

Device modelling. The theoretically accessible single-photon flux may be described by the figure of merit

$$N = \frac{\iint F_{\mathrm{p}}(\lambda,\sigma)\eta(\lambda,\sigma)I(\lambda)\mathrm{d}\sigma\mathrm{d}\lambda}{2\pi\int I(\lambda)\mathrm{d}\lambda}$$

where λ is the dipole wavelength and σ the dipole polarization. The Purcell factor $F_{\mathrm{p}} = \Gamma_{\mathrm{NW}}/\Gamma_{\mathrm{bulk}}$, which describes the modification of the NV centre fluorescence lifetime in a nanowire ($\tau_{\mathrm{NW}} = 1/\Gamma_{\mathrm{NW}}$) compared to the bulk ($\tau_{\mathrm{bulk}} = 1/\Gamma_{\mathrm{bulk}}$), was evaluated by comparing the total emitted power from a dipole in a diamond nanowire in a homogeneous diamond medium ($n = 2.4$). The collection efficiency η was calculated from the overlap of the dipole far-field pattern with the acceptance angle of our microscope objective (NA ≈ 0.95). To take into account the wavelength and polarization dependence of parameters F_{p} and η, they were averaged over the room-temperature NV centre fluorescence spectrum $I(\lambda)$, as well as over the (111) plane of a (100) diamond crystal. We calculated the figure of merit values for both nanowire ($N_{\mathrm{NW}} \approx 0.3$) and bulk ($N_{\mathrm{bulk}} \approx 0.03$) single-photon sources, and their ratio gives the order of magnitude improvement in single-photon flux due to nanostructuring. Note that in general F_{p} and η are sensitive to the radial position of the NV dipole owing to overlap with the nanowire mode and to axial position because of Fabry–Perot resonances formed between the nanowire facets. These effects may be responsible for the variation in nanowire brightness observed in Fig. 2c.

Received 27 October 2009; accepted 8 January 2010; published online 14 February 2010; corrected online 23 February 2010

References

1. Beveratos, A. *et al.* Single photon quantum cryptography. *Phys. Rev. Lett.* **89,** 187901 (2002).
2. Lounis, B. & Moerner, W. E. Single photons on demand from a single molecule at room temperature. *Nature* **407,** 491–493 (2000).
3. Englund, D. *et al.* Controlling the spontaneous emission rate of single quantum dots in a two-dimensional photonic crystal. *Phys. Rev. Lett.* **95,** 013904 (2005).
4. Högele, A., Galland, C., Winger, M. & Imamoğlu, A. Photon antibunching in the photoluminescence spectra of a single carbon nanotube. *Phys. Rev. Lett.* **100,** 217401 (2008).
5. Wang, C., Kurtsiefer, C., Weinfurter, H. & Burchard, B. Single photon emission from SiV centres in diamond produced by ion implantation. *J. Phys. B* **39,** 37–41 (2006).
6. Gaebel, T. *et al.* Stable single-photon source in the near infrared. *New J. Phys.* **6,** 98 (2004).
7. Aharonovich, I. *et al.* Two-level ultrabright single photon emission from diamond nanocrystals. *Nano Lett.* **9,** 3191–3195 (2009).
8. Kurtsiefer, C., Mayer, S., Zarda, P. & Weinfurter, H. Stable solid-state source of single photons. *Phys. Rev. Lett.* **85,** 290–293 (2000).
9. Beveratos, A. *et al.* Nonclassical radiation from diamond nanocrystals. *Phys. Rev. A* **64,** 061802(R) (2001).
10. Jelezko, F. *et al.* Observation of coherent oscillations in a single electron spin. *Phys. Rev. Lett.* **92,** 076401 (2004).
11. Prawer, S. & Greentree, A. D. Diamond for quantum computing. *Science* **320,** 1601–1602 (2008).
12. Gurudev Dutt, M. V. *et al.* Quantum register based on individual electronic and nuclear spin qubits in diamond. *Science* **316,** 1312–1316 (2007).
13. Neumann, P. *et al.* Multipartite entanglement among single spins in diamond. *Science* **320,** 1326–1329 (2008).
14. Maze, J. R. *et al.* Nanoscale magnetic sensing with an individual electronic spin in diamond. *Nature* **455,** 644–648 (2008).
15. Balasubramanian, G. *et al.* Nanoscale imaging magnetometry with diamond spins under ambient conditions. *Nature* **455,** 648–652 (2008).
16. Park, Y.-S., Cook, A. K. & Wang, H. Cavity QED with diamond nanocrystals and silica microspheres. *Nano Lett.* **6,** 2075–2079 (2006).
17. Larsson, M., Dinyari, K. N. & Wang, H. Composite optical microcavity of diamond nanopillar and silica microsphere. *Nano Lett.* **9,** 1447–1450 (2009).
18. Fu, K.-M. C. *et al.* Coupling of nitrogen-vacancy centers in diamond to a GaP waveguide. *Appl. Phys. Lett.* **93,** 234107 (2008).

19. Barclay, P. E., Fu, K.-M. C., Santori, C. & Beausoleil, R. G. Chip-based microcavities coupled to nitrogen-vacancy centers in single crystal diamond. *Appl. Phys. Lett.* **95,** 191115 (2009).
20. Kolosev, R. *et al.* Wave–particle duality of single surface plasmon polaritons. *Nature Phys.* **5,** 470–474 (2009).
21. Wang, C. F. *et al.* Fabrication and characterization of two-dimensional photonic crystal microcavities in nanocrystalline diamond. *Appl. Phys. Lett.* **91,** 201112 (2007).
22. Lee, C. L. *et al.* Fabrication and characterization of diamond micro-optics. *Diamond Rel. Mater.* **15,** 725–728 (2006).
23. Wang, C. F., Hu, E. L., Yang, J. & Butler, J. E. Fabrication of suspended single crystal diamond devices by electrochemical etch. *J. Vac. Sci. Technol. B* **25,** 730–733 (2007).
24. Fairchild, B. A. *et al.* Fabrication of ultrathin single-crystal diamond membranes. *Adv. Mater.* **20,** 4793–4798 (2008).
25. Hiscocks, M. P. *et al.* Diamond waveguides fabricated by reactive ion etching. *Opt. Express* **16,** 19512–19519 (2008).
26. Hausmann, B. *et al.* Fabrication of diamond nanowires for quantum information processing applications. Preprint at <http://arXiv.org/abs/0908.0352> (2009).
27. Friedler, I. *et al.* Solid-state single photon sources: the nanowire antenna. *Opt. Express* **17,** 2095–2110 (2009).
28. Epstein, R. J., Mendoza, F. M., Kato, Y. K. & Awschalom, D. D. Anisotropic interactions of a single spin and dark-spin spectroscopy in diamond. *Nature Phys.* **1,** 94–98 (2005).
29. Gali, A., Fyta, M. & Kaxiras, E. *Ab initio* supercell calculations on nitrogen-vacancy center in diamond: electronic structure and hyperfine tensors. *Phys. Rev. B* **77,** 155206 (2008).
30. Manson, N. B., Harrison, J. P. & Sellars, M. J. Nitrogen-vacancy center in diamond: model of the electronic structure and associated dynamics. *Phys. Rev. B* **74,** 104303 (2006).

Acknowledgements

The authors would like to thank F. Huber for providing Fig. 1b. Helpful discussions with Q. Quan, E. Togan, I. Bulu, M. Lukin and F. Jelezko are acknowledged. We would also like to thank S. Hong, M. Grinolds, P. Maletinsky and A. Yacoby for confirmation of the ESR signal. Devices were fabricated in the Center for Nanoscale Systems (CNS) at Harvard. This work was supported in part by grants from National Science Foundation (awards ECCS-0708905 and PHY-0646094: Nanoscale Science and Engineering Center and ECCS-0708905) and the Defense Advanced Research Projects Agency (Quantum Entanglement Science and Technology program). T.B. is funded by the NDSEG and NSF fellowships.

Disclaimer

The views, opinions and/or findings contained in this publication are those of the author and should not be interpreted as representing the official views or policies, either expressed or implied, of the Defense Advanced Research Projects Agency or the Department of Defense.

Author contributions

T.B. performed the experiments and analysed the data, B.H. and M.K. fabricated the diamond nanowire devices, and Y.Z. performed numerical modelling of the structure. J.M. contributed experimental tools and helped with the experiments. P.R.H. and M.L. conceived and designed the experiments. T.B. and M.L. wrote the paper. All authors discussed the results and commented on the manuscript.

Additional information

The authors declare no competing financial interests. Reprints and permission information is available online at http://npg.nature.com/reprintsandpermissions/. Correspondence and requests for materials should be addressed to M.L.